Title: Morphological and functional variability in central and subcentral motor cortex of the human brain

Abbreviated title: Variability in central and subcentral motor cortex

Authors: Nicole Eichert[1,*], Kate E. Watkins[2], Rogier B. Mars[1,3] & Michael Petrides[4,5]

[1] Wellcome Centre for Integrative Neuroimaging, Centre for Functional MRI of the Brain (FMRIB), Nuffield Department of Clinical Neurosciences, John Radcliffe Hospital, University of Oxford, OX3 9DU, Oxford, United Kingdom
[2] Wellcome Centre for Integrative Neuroimaging, Department of Experimental Psychology, University of Oxford, OX2 6GG, Oxford, United Kingdom
[3] Donders Institute for Brain, Cognition and Behaviour, Radboud University Nijmegen, 6525 AJ Nijmegen, The Netherlands
[4] Department of Neurology and Neurosurgery, Montreal Neurological Institute and Hospital, McGill University, 3801 University Street, Montreal H3A 2B4, QC, Canada
[5] Department of Psychology, McGill University, 1205 Dr. Penfield Avenue, Montreal H3A 1B1, QC, Canada

* **Corresponding author**: nicole.eichert@psy.ox.ac.uk

Number of pages: 40
Number of figures: 9
Number of tables: 3
Number of words for abstract: 161
Number of words for introduction: 646
Number of words for discussion: 1499

Conflict of interest: The authors declare no competing financial interests.

Acknowledgments:
N.E. is a Wellcome Trust Doctoral student in Neuroscience at the University of Oxford [203730/Z/16/Z]. N.E. was supported by a Lazlo and Etelka Kollar Brain@McGill Graduate/Postgraduate Travel Grant awarded by the Oxford McGill Zürich Partnership in the Neurosciences. The project was supported by the NIHR Oxford Health Biomedical Research Centre. The Wellcome Centre for Integrative Neuroimaging is supported by core funding from the Wellcome Trust [203139/Z/16/Z]. The work of R.B.M. is supported by the Biotechnology and Biological Sciences Research Council (BBSRC) UK [BB/N019814/1] and the Netherlands Organization for Scientific Research NWO [452-13-015]. The work of M.P is supported by CIHR Foundation Grant FDN-143212.

Abstract

There is a long-established link between anatomy and function in the somatomotor system in the mammalian cerebral cortex. Morphology of the central sulcus predicts the location of functional activation peaks in individuals, but morphological variation in the subcentral region and its relationship to functional activation is unknown. Investigating the subcentral region is particularly important in the context of speech, since control of the larynx during human speech production activates this region. Here, we examined whether morphological variation in the central and subcentral region is related to functional activation during movement of the hand, lips, tongue, and larynx at the individual subject level. We provide a systematic description of the sulcal pattern of the subcentral and adjacent opercular cortex, including the inter-individual variability of sulcal morphology. We found a robust relationship between morphology of the central and subcentral sulcal segments and movement of different effectors. A surface registration based on sulci revealed that anatomical variability explains, in part, spatial variability in function.

Significance Statement

There is a long established relationship between structure and function in the somatomotor system in the mammalian brain. Here, we show that the location of brain activations during movement involving different effectors relates to morphological landmarks in the central sulcus and the subcentral region of the cerebral cortex. We provide a systematic description of the morphological patterns of the subcentral cortical region and the inter-individual

anatomical variability of sulcal segments. We discuss how structural variability can explain spatial variability in functional activations, which is a critical factor for cross-subject registrations in group studies.

Introduction

A fundamental challenge in neuroscience is to establish meaningful links between brain function and structure. One of the clearest cases of such a structure-to-function relationship is found in the somatomotor system in the central strip of the cerebral cortex (Jackson, 1863; Hitzig and Fritsch, 1870; Vogt and Vogt, 1919; Penfield and Boldrey, 1937). Different parts of the body are represented in an orderly and consistent fashion, following a somatotopic organization, the schematic visualization of which is known as Penfield's 'homunculus'.

In contrast to electrical brain mapping studies, neuroimaging studies typically report average activations from larger groups. This approach demonstrates effects, which are representative of the human brain in general, but obscures subject-specific features and inter-individual variability, limiting sensitivity and functional resolution (Bennett and Miller, 2010; Nieto-Castañón and Fedorenko, 2012; Woo et al., 2014). Thus, a growing number of neuroimaging studies now tend to report activation patterns in individuals (Miller et al., 2002; Barch et al., 2013; Carey et al., 2017). A deeper understanding of structure-to-function relationships, however, requires examination of inter-individual functional variability together with anatomical variability.

Several studies have established a coupling between the sulcal/gyral brain anatomy and functional activation in individuals (e.g., Amiez et al., 2006; Derrfuss et al., 2012; Amiez et al., 2013; Zlatkina et al., 2016; Bodin et al., 2018). A recent neuroimaging study demonstrated that individual fMRI activation peaks showed a consistent relationship between the effector being moved and the morphologically defined segments of the central sulcus (Germann et al., 2019). The inter-individual variability of the central sulcus segments, however, was not quantified and this investigation focused exclusively on the central sulcus.

Movement representation in the human brain, however, is not limited to the central sulcus. The subcentral gyrus, in addition to the ventral region of the central sensorimotor strip, is involved in speech-related movements (Penfield and Boldrey, 1937; Olthoff et al., 2008; Grabski et al., 2012; Bouchard et al., 2013). Voluntary control of laryngeal movements during vocalization evokes brain activity in two distinct regions in lateral motor cortex: a dorsal region close to the representation of the lips and a ventral region close to the lateral fissure (reviewed in: Belyk and Brown, 2017; Eichert et al., 2020a). The representation of the larynx in the human brain, however, remains controversial and inconsistent reports in the literature might relate to inter-individual variability. Examining functional anatomy of the speech motor system thus requires investigation both of the central sulcus and the subcentral gyral region at an individual subject level.

There has been no systematic examination of the morphological variability in the subcentral gyrus and the adjacent opercular cortex. There are two distinct sulci in the subcentral region: the anterior subcentral sulcus (*ascs*) and the posterior subcentral sulcus (*pscs*) (Petrides, 2012, 2019). The variability of these two sulci in relation to the central sulcus segments across

111 individuals requires examination, as well as the relationship of morphological variability to
112 functional brain activity during movement.
113
114 Here, we assessed the structure-to-function relationship in the human motor system on an
115 individual subject level by examining the morphology of the central sulcus, the subcentral gyrus
116 and the adjacent central operculum. We performed sulcal labelling in surface space, rather
117 than in volume space, which is a suitable representation of the intrinsic topology of the
118 cerebral cortex (Fischl et al., 1999). To visualize and quantify inter-individual variability of the
119 examined sulcal segments, we derived spatial probability maps in both standard surface and
120 volume space. In a subset of subjects, we acquired fMRI data to localize brain activity during
121 movement of the hand, lips and tongue, as well as the larynx during vocalization (Eichert et al.,
122 2020a). To investigate how this structure-to-function relationship can help to improve
123 alignment of data, we registered all subjects based on the sulcal surface labels. A decrease in
124 distances across activation peaks after applying the registration indicates that anatomical
125 variability can explain some of the functional variability.
126
127
128 # Material and Methods
129
130 *Subjects*
131
132 Data from two groups of subjects were used. In one study group, both structural and functional
133 MRI data were acquired; in the other study group, only structural MRI data were available.

Structural and functional MRI data from the performance of motor tasks were acquired from 20 subjects (12 females, 18 – 40 years, 5 left-handers). All subjects were self-reported native English speakers (two were raised bilingually from infancy and three were fluent in a second acquired language) and had no history or diagnosis of speech disorders. All had normal hearing, normal or corrected-to-normal vision, and no neurological impairments. The subjects were part of a study that had been approved by the Central University Research Ethics Committee of the University of Oxford (CUREC, R55787/RE001) in accordance with the regulatory standards of the Code of Ethics of the World Medical Association (Declaration of Helsinki). All subjects gave informed consent for their participation and were monetarily compensated for their participation.

In addition, we used cortical brain surface reconstructions from 30 subjects provided by the Human Connectome Project (HCP), WU-Minn Consortium (Principal Investigators: David Van Essen and Kamil Ugurbil; 1U54MH091657) funded by the 16 NIH Institutes and Centers that support the NIH Blueprint for Neuroscience Research; and by the McDonnell Center for Systems Neuroscience at Washington University (Van Essen et al., 2013). The minimally pre-processed datasets of the first 31 subjects (16 female, age range 22-35 years) of the Q2 release were used. One subject was excluded because of a technical problem in the automatic FreeSurfer parcellation.

MRI Data Acquisition

MRI data acquisition parameters differed for the two groups of subjects. Data from the subjects that took part in the functional study were obtained at the Oxford Centre for Human Brain Activity (OHBA) using a 3T Siemens Prisma scanner with a 32-channel head coil. Two structural images of the whole brain had been acquired at 1 mm isotropic resolution; a T1w image (MPRAGE sequence) and a T2w image (SPACE sequence). For task-fMRI, whole head T2*-weighted echo planar images were acquired at 2.4 mm^3 isotropic resolution (TE = 30 ms, multiband fact 6, TR = 0.8 s, Casey et al., 2018).

Data acquisition and preprocessing methods of the HCP subjects are detailed in Glasser et al. (2013) and Uğurbil et al. (2013). T1w images had been acquired using an MPRAGE sequence at 0.7 mm isotropic resolution.

Experimental Design

The 20 subjects who provided structural and functional data took part in an fMRI study on speech production and laryngeal motor control. The experimental design, processing, and fMRI results of this study have been reported elsewhere in detail and are here only briefly described (Eichert et al., 2020a). In a functional localizer task, subjects were asked to perform repeated lip protrusion or tongue retraction at a rate of approximately 1-2 reps/s. The subject's breathing pattern was explicitly controlled using the fixation symbol on the screen, instructing them to inhale for 1.5 s and exhale for 4 s. A 'breathing only' condition, during which the subjects followed the same breathing pattern, was acquired as baseline condition. Each task condition was performed in blocks lasting 22 s followed by a rest period of 8 s with normal breathing. The conditions were presented in a fixed pseudo-random order following a balanced Latin-square design wherein each condition was repeated four times.

In a separate task, subjects were instructed to produce a syllable sequence (/la leɪ li la leɪ li/) under four different conditions: overt speech, silent mouthing, only vowel production and covert speech. Breathing instructions, task timing and randomization of the four blocks were the same as described for the localizer task, except that each condition was repeated five times. In a third task, subjects performed a phonological and semantic judgement task, which involved button presses with the right index finger to indicate responses. This task was analyzed as a localizer for the hand region in the left hemisphere.

Structural MRI Data Analysis

Data of the subjects who took part in the functional study were pre-processed using the HCP-pipeline Glasser et al. (2013). The automatic processing pipeline includes cortical surface reconstruction using FreeSurfer based on the contrast from the T1w and the T2w images and automatic assignment of neuroanatomical labels. Cortical surface reconstructions of the HCP subjects were derived using FreeSurfer based on the T1w scans and directly provided by the database. A linear transformation (12 degrees of freedom) from FreeSurfer's anatomical to standard MNI space (nonlinear 6th generation atlas, Fonov et al., 2011) was derived using FSL's FLIRT (Jenkinson and Smith, 2001; Jenkinson et al., 2002).

Functional MRI Data Analysis and Statistical Analysis

Functional MRI data processing was carried out using FEAT (FMRI Expert Analysis Tool) Version 6.00, part of FSL (FMRIB's Software Library, www.fmrib.ox.ac.uk/fsl) including motion correction of the images and unwarping using a fieldmap (Jenkinson, 2003). Time-series statistical analysis was based on a general linear model (GLM) implemented in FILM with local autocorrelation correction (Woolrich et al., 2001). Standard motion correction parameters and individual volumes that were motion outliers, determined using fsl_motion_outliers, were included as separate regressors at the first level for each subject. Registration to the high-resolution structural scan and standard 2-mm MNI template was carried out using FLIRT. Registration from high resolution structural to MNI space was then further refined using FNIRT nonlinear registration (Andersson et al., 2007).

In the functional localizer task for lip and tongue movement, activity during each condition was assessed relative to the 'breathing only' condition. For the syllable production task, the conditions were analyzed in a factorial model that allowed separation of the (supralaryngeal) articulation and the (laryngeal) vocalization components of the task. We refer to the latter as 'vocalization' component (index for laryngeal activity during voice production), while other studies have referred to it as voicing or phonation. Brain activity associated with the control of supralaryngeal articulation was defined as ('overt speech' *minus* 'vowel production') *plus* ('silent mouthing' *minus* 'covert speech') and the main contrast for vocalization was derived by the contrast ('overt speech' *minus* 'silent mouthing') *plus* ('vowel production' *minus* 'covert speech'). In both tasks described above, the rest blocks with normal breathing served as baseline, which means that they were not modelled in the GLM. For the hand localizer task, we derived a contrast of all conditions involving button presses relative to a resting baseline.

Individual Surface Activation Maxima

Activation maxima were derived using the steps described in Eichert et al. (2020a), which are repeated here. To assess intra-individual variability of the fMRI results, we derived the location of individual activation maxima for hand, lip, and tongue movement, and larynx activity during vocalization. Activation maxima were derived in both hemispheres in volume space using anatomically defined ROIs. For hand (left hemisphere only), lip, and tongue movement, we used the central sulcus as a volumetric ROI to extract the maximum. The ROI was defined using FreeSurfer's automatic volumetric labelling based on the Destrieux Atlas.

For the vocalization contrast from the syllable production task, which indicates laryngeal activity during voice production, we derived two separate activation maxima: one located in a dorsal area and one in a ventral area of the central sulcus. To account for additional articulation of the tongue during the syllable production task, a spherical ROI (7 voxels diameter) around each individual's maximum voxel from the tongue movement localizer was masked out from the *z*-statistics image of the vocalization contrast prior to extracting the maximum.

For the dorsal larynx ROI, we used a dorsally and ventrally cropped section of the central sulcus in volume space (coordinates in MNI space: $z = 50$ to $z = 30$). The ventral larynx ROI was derived manually based on individual anatomy in surface space to ensure that the ROI did not overlap with unrelated brain areas such as the subjacent auditory cortex in the temporal lobe or inferior frontal cortex located anteriorly. A liberal surface ROI was drawn on the individual's midthickness surface covering the ventral part of the central sulcus and adjacent gyri. Anteriorly, the ROI was delineated by the inferior portion of the precentral sulcus and posteriorly the ROI spanned the postcentral gyrus. If present, the lateral portion of the ascending sulcus in subcentral gyrus was included within the ROI. The dorsal limit of the ROI was defined by a horizontal line across the gyrus at the level of the usual location of the posterior ramus of the inferior precentral sulcus. The ventral larynx surface ROI was converted into a volumetric ROI covering the underlying cortical ribbon using Workbench Command (wb_command, www.humanconnectome.org/software/connectome-workbench.html).

Individual volumetric ROIs were linearly transformed from FreeSurfer's anatomical to functional space of the respective task fMRI scan. Within the ROI, the voxel of maximal intensity was determined from the *z*-statistics image. The activation maxima were mapped to

267 the individual's native midthickness surface, then smoothed (FWHM = 1 mm) and binarized to
268 form a small circular patch. To assess spatial variability of the functional activity, all subjects'
269 activation peaks were resampled to the same regular 32k surface mesh, prior to any
270 registration.
271
272
273 *Sulcal Labelling*
274
275 We identified the following sulci and sulcal segments in the structural data from all 50 subjects:
276 five segments of the central sulcus from dorsal to ventral (*cs_1* to *cs_5*), the lateral and
277 opercular segments of the anterior subcentral sulcus (*ascs_lat, ascs_op*) and the posterior
278 subcentral sulcus (*pscs*). Sulcal labels for one example subject are shown in Figure 1. Sulcal
279 labels were drawn manually onto the native surface mesh (approximately 136,000 vertices) in
280 Connectome Workbench's wb_view (www.humanconnectome.org/software/connectome-
281 workbench.html). Surface features of both pial and white matter surface were inspected in
282 conjunction with the subject's T1w scan. The identification of central sulcus segments was
283 based on changes in direction of the sulcus and on gyral 'plis de passage', which are small gyral
284 bridges connecting the postcentral with the precentral gyrus. These gyral bridges can be most
285 easily identified on the white matter surface (Germann et al., 2019).
286

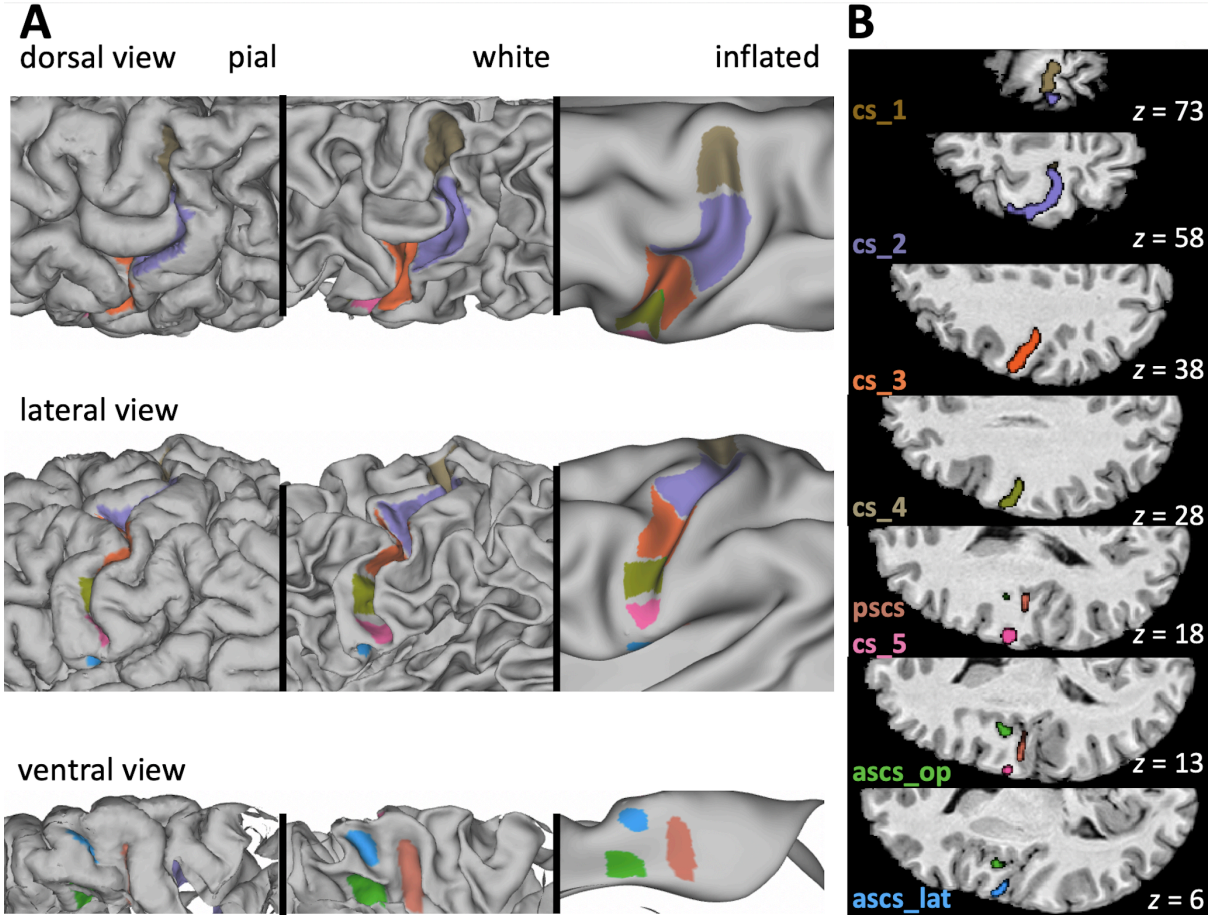

Figure 1: Sulcal labelling. **A**: Sulcal labels in one individual displayed onto the native pial surface, white matter surface, and inflated surface. **B**: Sulcal labels of the same subject in MNI volume space.

Cs_1 is the most dorsal segment of the central sulcus, which runs more or less in a vertical straight direction. Its ventral boundary was drawn at the location where a gyral bridge forms a prominent landmark on the posterior bank of the central sulcus. *Cs_2* has a characteristic curvature in the shape of the Greek omega letter (see Figure 1B), which is known as the 'hand knob' (Yousry et al., 1997). This knob is often more pronounced in the left hemisphere and it can comprise two smaller knob-like curves instead of one. The boundary between *cs_2* and *cs_3* was drawn at the location where the central sulcus changes direction and where a gyral passage can be observed on the posterior bank. In some subjects, an additional convexity of

the central sulcus can be observed on the posterior bank in the middle of *cs_3*. The ventral boundary of *cs_3* was drawn ventral to this convexity, at the location where a small gyral bridge forms a landmark on the anterior bank of the central sulcus. The last two segments of the central sulcus, *cs_4* and *cs_5* are smaller in extent, shallower and more variable in their morphology. The boundary between *cs_4* and *cs_5* was defined based on a gyral bridge on the posterior bank of the central sulcus. *Cs_5* is the most ventral part of the central sulcus, which can form an additional curve or run in straight direction.

The labels for *ascs* and *pscs* were assigned based on an atlas of human brain morphology (Petrides, 2019). For *ascs*, we labelled two distinct segments: a lateral and an opercular segment (*ascs_lat, ascs_op*). The course of *ascs_lat*, *ascs_op* and *pscs* was found to be highly variable and a detailed description of the sulcal anatomy in the subcentral region is reported in the results section.

The morphological patterns of the ventral subcentral region were categorized into five types depending on the configuration of *ascs_lat*. The classification was based on the location of *ascs_lat* on the cortex and its spatial relation to other sulci. Sulcal segments were considered as 'merged', when there was a clear continuation on the pial surface, although, in some cases, a discontinuity between the merged sulci was still observed on the white matter surface.

Spatial Probability Maps

In order to characterize the inter-individual morphological variability of the labelled sulci, we generated probability maps in surface and volume space. To obtain surface probability maps, all surface labels were resampled from native to a common regular 164k mesh. At each vertex, the 50 binary surface maps were summed and then normalized to create a surface label with intensities ranging from 0 % to 100 % at the maximal possible overlap of all 50 subjects. For visualization, the surface probability maps were displayed onto the average of all subjects' inflated surfaces.

For the generation of volumetric probability maps, we first deformed the subjects' native pial surface to MNI space by applying a linear transformation (12 degrees of freedom). Then we mapped the surface labels from the pial surface to 0.5 mm resolution volume space using wb_command. The individual volumetric labels were smoothed (Gaussian kernel with FWHM of 2 mm), thresholded at 0.1, binarized and then summed at each voxel. For visualization, volume probability maps were overlaid onto the 0.5 mm MNI average brain.

Structure-to-Function Relationship

Next, we examined the spatial relationship between the sulcal segments and the task activation peaks at the individual subject level. This analysis was performed in the 20 subjects who contributed both task and structural data. Individual task activation peaks were mapped onto the individual's cortical surface as described above for sulcal segments. As Extended Data (Figure 6-1), we show sulcal labels and activation peaks for all subjects, which allows an assessment of the spatial relationships at the individual subject level.

In order to characterize the structure-to-function relationship at the group level, we aligned all individual surfaces based on the anatomical surface labels and then we applied the same registration to individual task activation peaks. This approach allowed us to visualize individual variability in the spatial distribution of task activation peaks in a common group-level space.

The registration of sulcal labels was driven by the binary labels for *cs_1*, *cs_2*, *cs_3*, *cs_4*, *cs_5*, *ascs_lat, ascs_op* and *pscs* and performed using multimodal surface matching (MSM, Robinson et al. (2014). As target, or reference, for the MSM-based registration, we used the normalized and thresholded (> 0.4) average labels after projecting all of them to the same regular sphere (approximately 32,000 vertices). Each subject's sulcal maps and the reference sulcal maps were merged into a combined file with six data arrays. Then, we derived a registration using MSM for each subject. We refer to the average of the transformed labels resulting from the MSM registration as 'group-level segments'.

To characterize the structure-to-function relationship, we quantified the effect of the registration on the spatial variability of the activation peaks. The spatial variability of peaks in each task cluster before and after applying the registration was quantified by computing the median geodesic distances across all 20 activation peaks for each effector on a regular sphere. We compared this measure to a baseline measure of spatial variability prior to any anatomical registration, where the functional peaks were resampled to a common sphere. We also derived two additional anatomical registrations using the same steps as described above: one using the identical parameters, but based on four FreeSurfer labels (precentral gyrus, central sulcus, postcentral gyrus, subcentral gyrus/sulcus) and one based on sulcal depth whole-brain maps

using MSM default settings. FreeSurfer labels and sulcal depth maps were provided by the HCP-processing pipeline.

Results

Sulcal Pattern of the Subcentral Region

The sulcal anatomy of the subcentral region was examined in a total of 100 hemispheres (*n* = 50 brains) and the morphological patterns encountered were classified into five types (Figure 3). The most commonly observed configuration of subcentral sulci (Type 1, 44 % of hemispheres) is shown in Figure 2. The example in Figure 1 also shows an individual hemisphere classified as Type 1. In the Type 1 configuration, the central sulcus does not extend ventrally to meet the lateral fissure. The fifth and most ventral segment of the central sulcus (*cs_5*) is typically short and forms a curve in an anterior direction. The lateral segment of *ascs* (*ascs_lat*) is visible on the lateral surface of the brain and is clearly separate from the central sulcus. Dorsally, the *ascs_lat* extends into the precentral gyrus with variable length. Ventrally, the *ascs_lat* continues into the opercular cortex, which is hidden within the lateral fissure of the brain. A small gyral bridge separates the *ascs_lat* from the opercular segment of *ascs* (*ascs_op*), which continues medially until it reaches the circular insular sulcus (*cris*). The medial origin of the *ascs_op* can be identified at a curve of *cris*, which is formed by the posterior short insular gyrus just anterior to the central insular sulcus (*cis*). Posterior to *ascs_op*, the posterior subcentral gyrus (*pscs*) can be found, which extends laterally towards the lateral fissure. The

392 medial origin of *pscs* can be identified at a curve of *cris* posterior to *cis*, which is formed by the
393 anterior long insular gyrus. The number of curvatures of *cris* and the number of subcentral
394 sulci is variable, but the *ascs_op* and the *pscs* could be reliably identified in every subject
395 examined. The morphology of all of the mentioned sulci is variable across subjects, but the
396 description of morphological sub-types below focusses on the configuration of the *ascs_lat*.
397

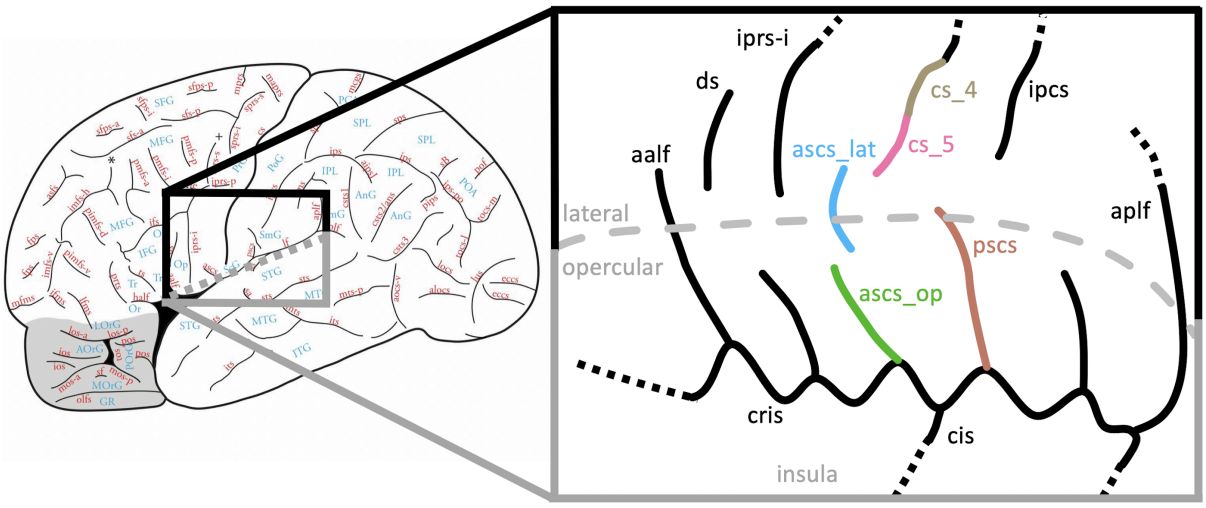

398

399 Figure 2: Sulcal pattern of the subcentral region. **Left**: Sulcal map of the human cerebral cortex
400 (Petrides, 2012). **Right**: Type 1 configuration of sulci in the subcentral region. Anatomical variability was
401 assessed in the sulci marked with colour: *ascs_lat*, lateral segment of the anterior subcentral sulcus;
402 *ascs_op*, opercular segment of the anterior subcentral sulcus; *cs_1* to *5*, segments of the central sulcus
403 (only *cs_4* and *cs_5* are shown in the highlighted region); *pscs*, posterior subcentral sulcus. Grey dashed
404 line: visible surface boundary between lateral and opercular cortex. *aalf*, ascending anterior ramus of
405 the lateral fissure; *aplf*, ascending posterior ramus of the lateral fissure; *cis*, central insular sulcus; *cris*,
406 circular insular sulcus; *ds*, diagonal sulcus; *iprs*, inferior precentral sulcus.

407
408
409 *Different Types of Morphological Patterns*
410

411 The subcentral region exhibits high inter-individual variability regarding the configuration of
412 the *ascs_lat*. The observed occurrences of morphological types are reported in Table 1. In
413 addition to the canonical (Type 1, 44 % of hemispheres) configuration described above, it was
414 commonly observed that the *ascs_lat* merged with the central sulcus (Type 2, 20 %) (Figure 2).
415 In these cases, the *ascs_lat* remains mostly on the lateral brain surface and does not reach into
416 the opercular cortex. The *ascs_op* extends further lateral and its extension is visible on the
417 lateral brain surface. Another commonly observed sub-type was identified by a more opercular
418 position of the *ascs_lat* (Type 3, 18 %). In Type 3, the *ascs_lat* is less visible on the lateral
419 surface and the central sulcus extends further ventral towards the lateral fissure. Type 3 is also
420 characterized by a reduced gyral bridge separating the *ascs_lat* from the *ascs_op*. In six cases,
421 the opercular continuation of the the *ascs_lat* curved posteriorly and merged with *pscs* instead
422 of the *ascs_op* (not shown as separate type). In several cases, we also observed the *ascs_lat*
423 to merge with the inferior ramus of the inferior precentral sulcus (*iprs-i*) (Type 4). When
424 *ascs_lat* and *iprs-i* merge, the ventral continuation of *ascs_lat* curves in an anterior rather than
425 a posterior direction and the position of *ascs_lat* is more lateral than opercular. In a few cases
426 (Type 5) the position of the *ascs_lat* was notably further rostral so that it was positioned
427 anterior to *ascs_op* rather than posterior as in the other configurations.
428
429 Strong hemispheric differences were observed in the occurrences of the morphological types
430 (Table 1). Type 2 (*ascs_lat* merged with *cs_5*) is much more common in left hemispheres (85
431 % vs. 15 %), while Type 4 (*ascs_lat* merged with *iprs*) and Type 5 (*ascs_lat* further anterior),
432 are more common in right hemispheres (75 % vs. 25 % for Type 4; 83 % vs. 17 % for Type 5),
433 although both types are infrequent. For Type 1 (canonical configuration) and Type 3 (*ascs_lat*
434 merged with *ascs_op*) no pronounced hemispheric differences were observed.

435

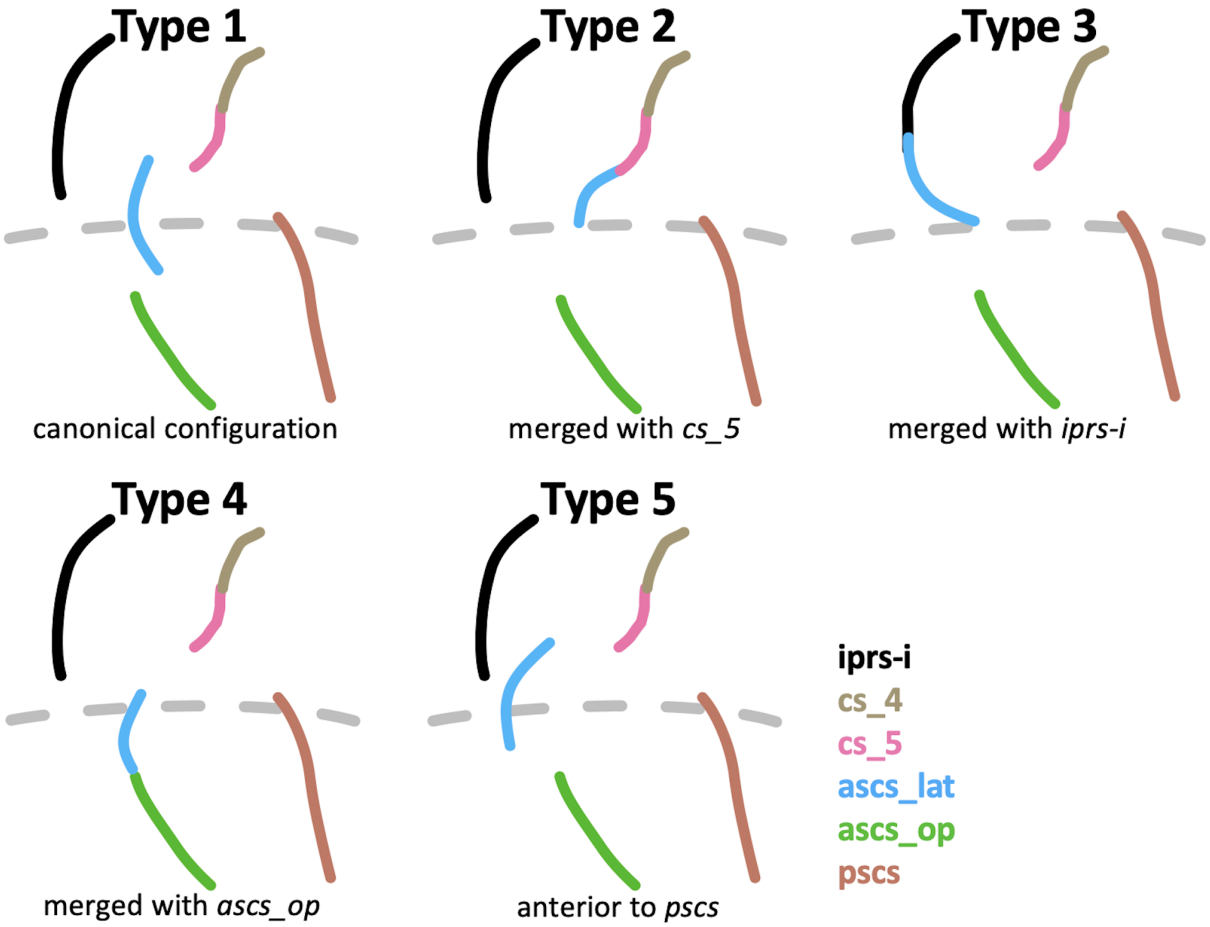

436

437 Figure 3: Morphological patterns. Schematic drawings illustrating the main morphological patterns of
438 the subcentral region formed by the *ascs_lat* with neighbouring sulci. Type 1: Canonical configuration
439 observed in the majority of hemispheres (also shown in Figure 2). Type 2: *ascs_lat* merged with the
440 central sulcus. Type 3: *ascs_lat* merged with *ascs_op*. Type 4: *ascs_lat* merged with the inferior ramus
441 of *iprs*. Type 5: *ascs_lat* anterior to *ascs_op*.

442

443 Table 1: Morphological patterns. Observed frequencies of morphological patterns based on 100
444 examined hemispheres (LH – left hemisphere; RH – right hemisphere).

	Type 1	Type 2	Type 3	Type 4	Type 5
LH	20	17	9	3	1

RH	24	3	9	9	5
Total	44	20	18	12	6

Spatial Probability Maps

The morphological variability of the central sulcus segments and the subcentral sulci was quantified and visualized using spatial probability maps in 2D surface space and 3D volumetric space (Figure 4, Figure 5). For both surface and volume probability maps, intensity values decrease from the center of the map towards the edges, which is typical for overlap maps. Maximal and median values of the probability maps are reported as Extended Data (Figure 4-1). Values in the volumetric probability maps are overall lower given that they capture variability in three spatial dimensions. The pattern of values across sulci and hemispheres, however, is consistent across surface and volumetric probability maps. For all sulci, hemispheric differences were observed with regard to the location in volume space (Figure 5). All sulcal segments in the left hemisphere are located consistently further posterior compared to the segments on the right hemisphere, which is in line with the Yakovlevian anticlockwise torque of the two hemispheres (see Table 2 for coordinates of the voxel of maximal probability and for the center of gravity for each label).

The first three segments of the central sulcus (*cs_1 - 3*) show high inter-individual spatial consistency, which is characterized by high values, i.e. overlap, in the probability maps. Consistency is lower for *cs_4* and *cs_5*. Consistency is also low for the subcentral sulci (*ascs_lat*, *ascs_op*, *pscs*) with lowest consistency for *ascs_lat*, especially in the left hemisphere. The

hemispheric effect for the *ascs_lat* is evident in both surface and volumetric probability maps. It was observed that the *ascs_lat* is larger in extent and deeper in the right hemisphere (see for example Figure 5, slice *y* = -1). The low consistency in *ascs_lat* is in line with the variable morphological subtypes that were described above. The two subcentral sulci, *ascs_op* and *pscs*, are less consistent than the central sulcus segments, but more consistent than the *ascs_lat*. *Ascs_op* and *cs_5* show a tendency for more variability in the right hemisphere, which is the opposite pattern of lateralization in comparison with that for the *ascs_lat*.

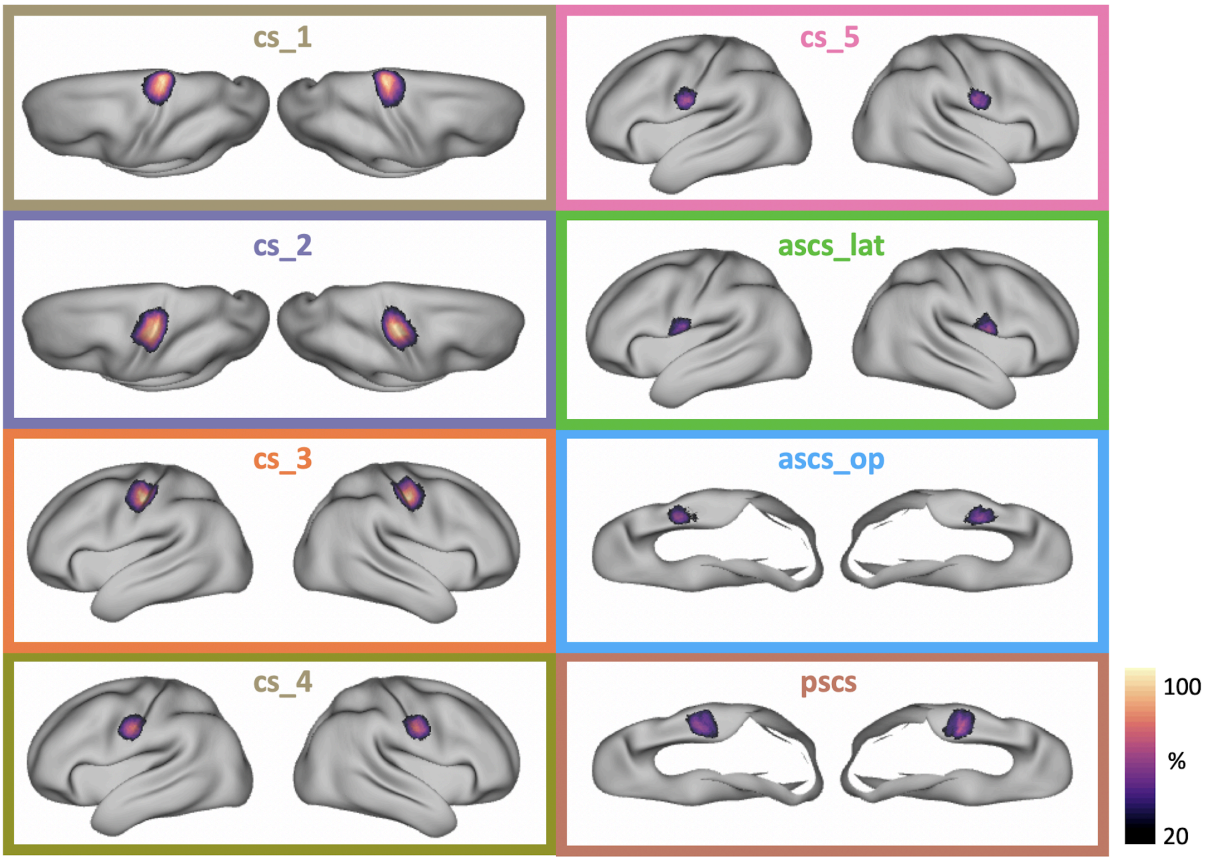

Figure 4: Surface probability maps. Probability maps of central and subcentral sulcal labels shown on an inflated average surface (*n* = 50). Labels for *cs_1* and *cs_2* are shown from a dorsal perspective. Labels for *ascs_op* and *pscs* are shown from a ventral perspective with the temporal lobe removed for better visibility of the opercular cortex. Intensity values show the amount of overlap with 100 % indicating an overlap in all subjects.

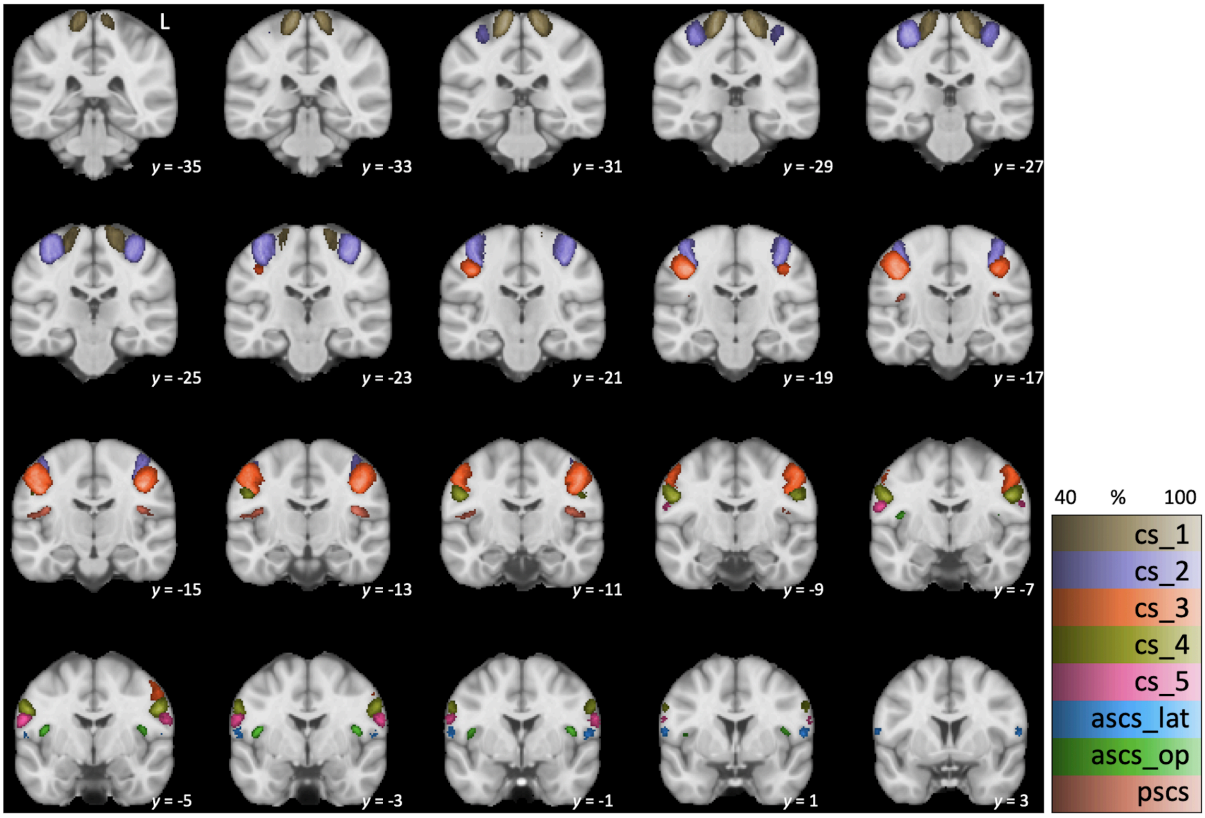

Figure 5: Volumetric probability maps. Probability maps generated after linear registration to MNI space overlaid onto the standard MNI template (n = 50). L – left hemisphere shown on right side of the image. Intensity values show the amount of overlap across subjects. Color maps for the different sulci have been matched in luminance so that darker colors indicate a lower overlap.

Table 2: Coordinates of probability maps. MNI-coordinates (*x, y, z*) of each sulcal segment's maximal voxel and the center of gravity in the volumetric probability maps.

		maximum			center of gravity		
	sulcus	*x*	*y*	*z*	*x*	*y*	*z*
left	*cs_1*	-14	-30	69	-17	-30	-69

	cs_2	-36	-26	58	-36	-24	59
	cs_3	-38	-18	42	-47	-15	46
	cs_4	-54	-8	30	-55	-7	32
	cs_5	-58	-6	22	-60	-4	22
	ascs_lat	-60	2	12	-58	0	12
	ascs_op	-41	-4	14	-44	-3	10
	pscs	-39	-16	18	-48	-14	15
right	*cs_1*	16	-28	68	18	-28	69
	cs_2	38	-23	60	36	-21	58
	cs_3	44	-14	40	48	-12	46
	cs_4	58	-4	32	56	-5	32
	cs_5	62	-2	21	62	-2	22
	ascs_lat	58	1	10	58	2	12
	ascs_op	42	-3	14	44	-2	11
	pscs	41	-14	18	48	-13	16

Sulcal Registration and Structure-to-Function Relationship

We registered all individual surfaces based on the binary sulcal labels using MSM. We then applied the registration to individual surface activation peaks from movement of different effectors. By these means, we could visualize and assess the spatial relationship of functional peaks to the sulcal labels at the group level. After registering the sulcal labels, we averaged all transformed sulcal labels and thresholded ($t > 0.4$) the average labels to obtain the outlines of

group-level sulcal segments. Figure 6A shows the outlines of thresholded group-level sulci, which demonstrates an orderly dorsal-ventral configuration of the sulcal segments.

Next, we applied the registration that was used to transform individual surface labels to the group space to the functional activation peaks of different effectors in individual subjects. Figure 6B-F shows the location of the resampled activation maxima in relation to the outlines of the group-level sulcal segments. Given that the same registration was applied to individual sulcal labels and the peaks, the location of resampled peaks with respect to the group-level sulci reflects the original spatial relationship on the native surfaces of the individuals.

Overall, a strong correspondence between sulcal labels and functional peaks was observed. The observed relationships between labels and peaks are reported in Table 3. The majority of activation peaks from the hand localizer fall inside the center of *cs_2*. The dorsal peaks for larynx activity are found on the anterior bank of *cs_3*. Peaks from the lip localizer also fall within *cs_3* and overlap with the location of the dorsal larynx peaks. Those for the lip, however, are reliably located at the more ventral extent of *cs_3* whereas those for the dorsal larynx peaks span the segment. Activation peaks from the tongue localizer fall inside *cs_4* with high consistency. The ventral peaks for larynx activity are associated with *cs_5* and *ascs_lat* or with the gyrus in between, but the relationship is less reliable than for the other functional peaks.

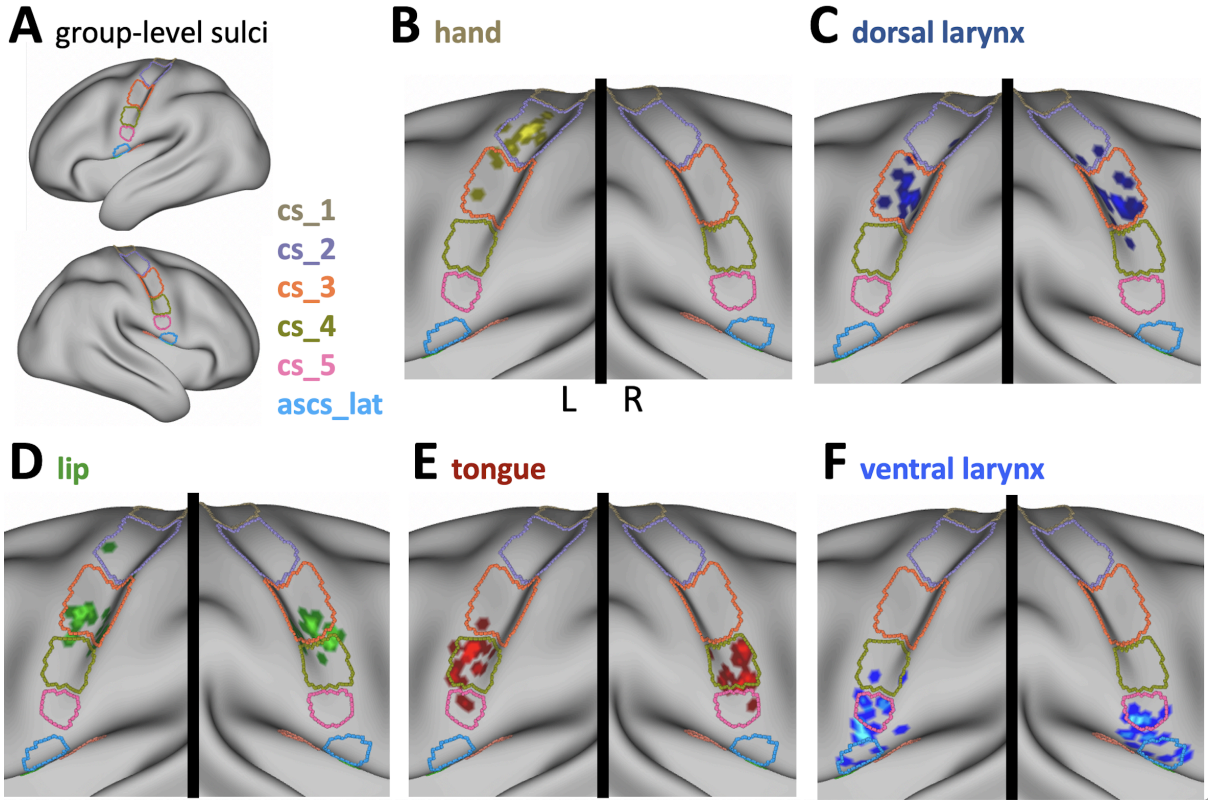

Figure 6: Structure-to-function relationships. **A**: Outlines of the averaged, normalized and thresholded (> 0.4) sulcal maps after registration using MSM (i.e. the group-level sulci). **B-F**: Location of individual activation peaks with respect to the sulcal maps after applying the sulcal registration (*n* = 20). Brighter colors indicate overlapping peaks. Only the central strip of the brain is shown.

Table 3: Structure-to-function relationships. Observed relationships between functional activation peaks and sulcal labels based on 40 examined hemispheres. The number of peaks for each effector are given for each sulcal segment.

	cs_1	*cs_2*	*cs_3*	*cs_4*	*cs_5*	*ascs_lat*
hand (only LH)	0	16	4	0	0	0
dorsal larynx	0	2	37	1	0	0
lip	0	1	34	5	0	0
tongue	0	0	1	36	3	0

ventral larynx	0	0	0	2	24	14

To characterize the effect of the sulcal registration on the spatial variability of functional peaks, we computed the median distance between all peaks for each effector before and after applying the sulcal transformation, which is shown in the Extended Data (Figure 6-2). Spatial variability decreased by 11 %, but not to the same extent for all effectors. Clusters in the left hemisphere benefitted more from the registration, but an exception is the left lip cluster, where values increased due to an outlier (see Figure 6D). A comparison with a registration based on FreeSurfer's automatic labels and by sulcal depth demonstrated that all three anatomical registrations decrease spatial variability when compared to baseline. Performance of the three registrations is similar across all effectors, but spatial variability of the left ventral larynx cluster decreased most using the sulcal label registration. Taken together, this quantification indicates that a registration based on anatomical information decreases the spatial variability of functional activation peaks. At the given sample size, however, the reported differences do not reach statistical significance.

Discussion

We examined the morphological patterns and the inter-individual variability of the sulci in the subcentral region of the cerebral cortex in the human brain and their relation to motor activity. A robust relationship between morphological features of central and subcentral sulcal

segments and movement of different effectors at the individual subject level was demonstrated. Cross-subject registration based on the individually drawn sulcal labels showed that morphological variability explains functional variability in part.

Morphology of the Subcentral Cortex and the Central Operculum

The present study provided a systematic examination of the sulcal patterns of the subcentral and adjacent opercular cortical region in the human brain, including inter-individual variability of the sulcal morphology. In this region, one encounters an anterior and a posterior subcentral sulcus (*ascs*, *pscs*) (Petrides, 2012, 2019). We showed that, in the majority of subjects, the *ascs* consists of a distinct lateral (*ascs_lat*) and a distinct opercular segment (*ascs_op*).

The morphological patterns of the subcentral region were classified into five distinct subtypes, based on the configuration of *ascs_lat*. In addition to the canonical configuration (Type 1, Figure 2), the *ascs_lat* often merged with the central sulcus, so that the central sulcus complex extended further ventral towards the lateral fissure (Type 2). In Type 3, the *ascs_lat* merges with the inferior precentral sulcus (*iprs*). In Type 4, the position of the *ascs_lat* is notably more opercular and it merges with the *ascs_op*, so that the *ascs_lat* and *ascs_op* form one continuous sulcus. Type 5 is characterized by a more anterior position of the *ascs_lat*, compared with its position in the other types. The variability in the configuration of the lateral and opercular segments explains why the *ascs* appears as one continuous sulcus in a volumetric average of structural brain images in MNI space (Petrides, 2019).

574

575 *Sulcal Labelling in Surface Space*

576

577 We labelled sulcal segments directly on the subject's native cortical surface, rather than in
578 volume space as traditionally done in several MRI-based labelling studies (Germann et al.,
579 2005, 2019; Zlatkina and Petrides, 2010; Amiez et al., 2013; Sprung-Much and Petrides, 2018,
580 2019). Surface space provides a parsimonious representation of the sheet-like geometry of the
581 cerebral cortex. We reproduced the segmentation of the central sulcus, as described in a
582 volumetric labeling study (Germann et al., 2019). The underlying morphological features are
583 easily visualized in surface space and the labelling is reproducible. Furthermore, using surface
584 labels allowed us to perform a surface-based registration, where distances are represented as
585 geodesic distances along the cortex rather than as Euclidean distances between voxels (Fischl
586 et al., 1999; Klein et al., 2010). In the current study, the labels were drawn manually, but future
587 research could develop automatic classification of sulcal segments based on supervised
588 learning algorithms (Clouchoux et al., 2006; Takerkart et al., 2015).

589

590

591 *Spatial Probability Maps*

592

593 We visualized the morphological variability and spatial extent of the central sulcus segments
594 and the subcentral sulci in surface and volumetric probability maps. The first three central
595 sulcus segments show the highest spatial consistency across subjects. Consistency decreases
596 for the fourth and even further for the most ventral (fifth) segment of the central sulcus, which
597 is in line with previous observations (Germann et al., 2019). The decrease in probability values

598 for *cs_4* and *cs_5* can also be attributed to their smaller spatial extent compared to the sulcal
599 labels for *cs_1-3*. Consistency for the subcentral sulci *ascs_lat*, *ascs_op* and *pscs* is also notably
600 reduced, which is in line with the inter-subject variability in the morphological patterns as
601 described above.
602
603
604 *Hemispheric Differences*
605
606 The classification of morphological subtypes and the spatial probability maps revealed
607 hemispheric differences in the subcentral cortex, indicating that the position of the *ascs_lat*
608 along the rostro-caudal axis differs between hemispheres, but the dorso-ventral position does
609 not. The *ascs_lat* in the left hemisphere tends to be located further posterior, which frequently
610 results in a merge with the central sulcus, while the *ascs_lat* in the right hemisphere is located
611 more anteriorly. The inter-individual variability as characterized in the spatial probability maps
612 showed that the *ascs_lat* is less variable and larger in extent in the right hemisphere.
613
614 These hemispheric differences can be interpreted in relation to sulcal variability of the ventro-
615 lateral cortex (Germann et al., 2005; Sprung-Much and Petrides, 2018, 2019). Language
616 processing is lateralized to the left hemisphere and the role of left inferior frontal cortex in
617 language function is widely established (Broca, 1861; Price, 2000; Vigneau et al., 2006; Hickok
618 et al., 2016). Functional language lateralization is associated with structural asymmetries
619 (Foundas et al., 1996; Josse and Tzourio-Mazoyer, 2004) and increased regional variability
620 (Croxson et al., 2018), but the structure-to-function relationships remain controversial
621 (Dorsaint-Pierre et al., 2006; Sprung-Much and Petrides, 2018). We presume that increased

surface area in the left inferior frontal cortex affects the neighboring sulci so that the *ascs_lat* is 'pushed' to a relatively further posterior position in the left hemisphere. Despite the hemispheric differences in morphology, the structure-to-function relationships for basic movements of different effectors described below, did not exhibit notable differences between hemispheres.

Functional Activation Peaks and Morphology

Here we demonstrated a tight link between individual morphological features of the cortex and activation peaks for the different effectors examined. We replicated the relationships between central sulcus segments and functional localizers for the hand, lip, tongue, and larynx described in Germann et al. (2019). The functional localizer for larynx activity in the current study differed substantially from the one used by Germann et al., where 'humming' was the task instruction. Furthermore, we identified two larynx peaks in each subject, because more recent studies suggest that two separate regions in the central motor strip correlate with larynx activity (Belyk and Brown, 2017; Jarvis, 2019; Eichert et al., 2020a). The ventral 'humming' peak in Germann et al. was associated with the fifth segment of the central sulcus. The current analysis, however, showed that the ventral larynx peak was also localized in the *ascs_lat* in a large portion of subjects. The difference across studies might be due to the significantly larger sample size in the current study, which allowed a more robust assessment of the relationships.

It should be noted that the functional contribution of both larynx regions in motor control during vocalization is still debated (Simonyan, 2014; Belyk and Brown, 2017). Quantifications

of cortical microstructure, such as myelin content, indicates that the ventral larynx region is not located in primary motor cortex (Eichert et al., 2020a). The focus of the current study, however, is not the interpretation of the functional activation peaks *per se* but the relationship between their location and the underlying morphology. The individual variability in the cortical location of the ventral larynx area could be one factor in explaining inconsistent reports in the literature.

Relationship between Variability in Structure and Function

Cross-subject registration based on anatomical features decreased the spatial variability of the functional peaks, indicating that anatomical variability explains some functional variability. The somatomotor system, however, is only one example system, where a link between sulcal morphology and function at the individual subject level was established (Boling et al., 1999; Coulon et al., 2011; Zlatkina et al., 2016; Germann et al., 2019). Detailed anatomical and functional studies have also revealed these relationships for other parts of the cortex (Amiez et al., 2006; Bodin et al., 2018).

A registration based on individually drawn sulci showed a better registration for the left ventral larynx area, when compared to a registration based on sulcal depth and based on FreeSurfer labels, which rely on prominent and consistent landmarks, such as deep sulci. This observation demonstrates that manual identification of anatomical features is particularly important to examine spatial morphology in variable brain regions that have low gyrification. Further work

669 on structural and functional registrations may reveal a more nuanced picture of which
670 combination of anatomical features can better predict functional activations.
671
672 In the current study, we examined gross-anatomical features of the brain surface, an approach
673 that is directly applicable to neuronavigation and neurosurgical planning. Recent advances in
674 neuroimaging, however, allow us to acquire multiple image modalities in the same subjects,
675 some of which correlate with the underlying cellular microstructure (Fischl and Dale, 2000;
676 Zhang et al., 2012; Weiskopf et al., 2013). Although the histological analysis of post-mortem
677 brains remains the gold standard to define anatomical parcels of the brain, neuroimaging has
678 become a versatile tool for parcellating the cortex and to establish relationships between
679 different modalities (Glasser et al., 2016; Jakobsen et al., 2018; Smith et al., 2019; Eichert et
680 al., 2020b). Future work will show how detailed morphological labelling and segmentation
681 studies can benefit from other neuroimaging modalities.
682
683 In summary, the current study demonstrated a robust relationship between morphological
684 features of the central and subcentral sulcal segments and movement of different effectors at
685 the individual subject level. We described the morphological patterns of the sulci in the
686 subcentral and central opercular cortical region and their inter-individual variability. Laryngeal
687 activity during vocalization activates the subcentral region, which we found to be highly
688 variable across participants. This variability could explain inconsistencies in previous reports
689 about a ventral larynx area.
690
691
692

Extended Data

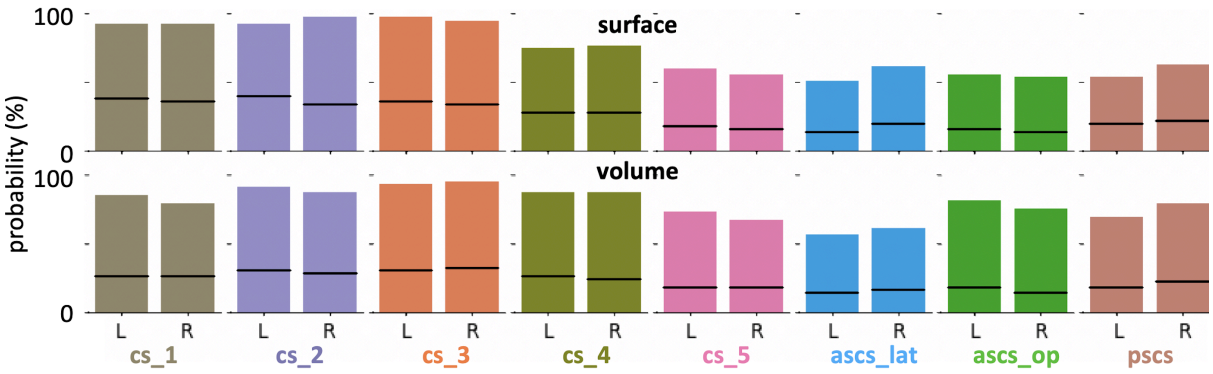

Figure 4-1: Quantification of probability maps. Bars show the maximal probability of overlap for sulcal labels in surface and volume space in the left (L) and right (R) hemisphere. Horizontal black lines indicate the median value of the probability map.

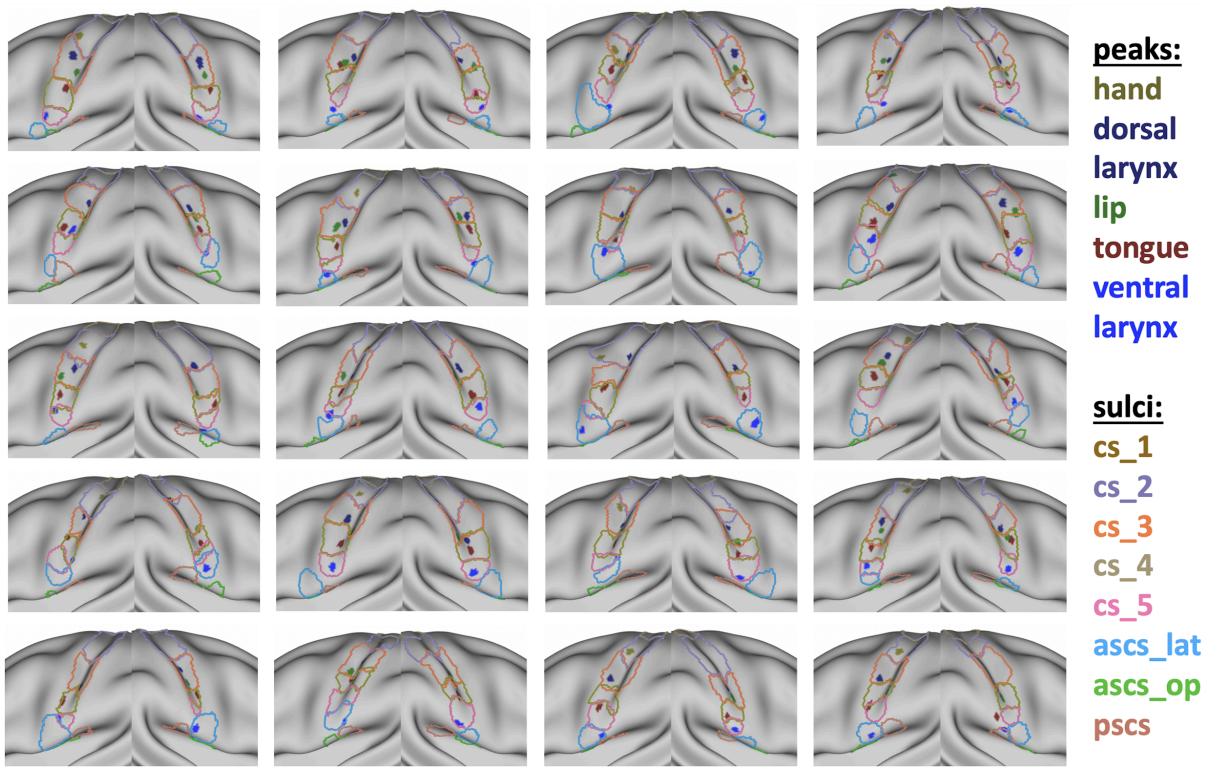

Figure 6-1: Individual sulcal labels and activation maxima. Data from the subset of subjects, where both anatomical and functional data were available.

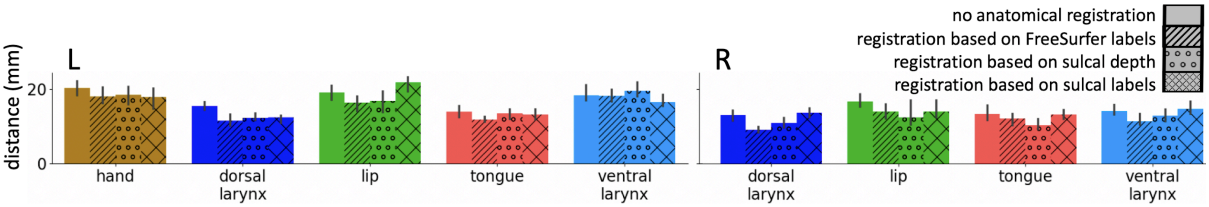

Figure 6-2: Effect of anatomical registrations on functional variability. Distance of task activation peaks prior to any anatomical registration (blank bars), after registration based on FreeSurfer labels (precentral gyrus, central sulcus, postcentral gyrus, subcentral gyrus/sulcus) (striped bars), after registration based on sulcal depth (dotted bars) and after registration based on manually drawn sulcal labels (crossed bars). The median distance ± 95% confidence interval is shown across all peaks for each task cluster (n = 20, 190 pairs of points for each cluster).

Author Contributions

Conception and design: NE, MP. Acquisition of data: NE, KEW. Analysis and interpretation of data: NE, KEW, RBM, MP. Original draft: NE, MP. Revising the article: NE, KEW, RBM, MP. Contribution of analytic tools: NE, RBM.

Data Accessibility

Upon acceptance of the manuscript, all derived data supporting the findings of this study will be made available from the Wellcome Centre for Integrative Neuroimaging's GitLab at git.fmrib.ox.ac.uk/neichert/project_variability. Anatomical raw data of the subjects that provided structural and functional data is publicly available at OpenNeuro under the accession code ds002634 (version 1.0.1). The minimally pre-processed data of the HCP subjects is openly available for download at https://db.humanconnectome.org.

Code and Software Accessibility

Upon acceptance of the manuscript, all processing code will be made available from the Wellcome Centre for Integrative Neuroimaging's GitLab at git.fmrib.ox.ac.uk/neichert/project_variability. FSL tools, including MSM, are available from fsl.fmrib.ox.ac.uk. Connectome Workbench is available at www.humanconnectome.org/software/connectome-workbench.html.

References

Amiez C, Kostopoulos P, Champod AS, Petrides M (2006) Local morphology predicts functional organization of the dorsal premotor region in the human brain. Journal of Neuroscience 26:2724–2731.

Amiez C, Neveu R, Warrot D, Petrides M, Knoblauch K, Procyk E (2013) The location of feedback-related activity in the midcingulate cortex is predicted by local morphology. Journal of Neuroscience 33:2217–2228.

Andersson JLR, Jenkinson M, Smith SM (2007) Non-linear optimisation FMRIB technial eport TR07JA1.

Barch DM et al. (2013) Function in the human connectome: Task-fMRI and individual differences in behavior. NeuroImage 80:169–189.

Belyk M, Brown S (2017) The origins of the vocal brain in humans. Neuroscience and Biobehavioral Reviews 77:177–193.

Bennett CM, Miller MB (2010) How reliable are the results from functional magnetic resonance imaging? Annals of the New York Academy of Sciences 1191:133–155.

Bodin C, Takerkart S, Belin P, Coulon O (2018) Anatomo-functional correspondence in the superior temporal sulcus. Brain Structure and Function 223:221–232.

Boling W, Olivier A, Bittar RG, Reutens D (1999) Localization of hand motor activation in Broca's pli de passage moyen. Journal of Neurosurgery 91:903–910.

Bouchard KE, Mesgarani N, Johnson K, Chang EF (2013) Functional organization of human sensorimotor cortex for speech articulation. Nature 495:327–332.

Broca P (1861) Remarques sur le siège de la faculté du langage articulé suivies d'une observation d'aphemie. Bull Soc Anthropol 6:330–357.

759 Carey D, Krishnan S, Callaghan MF, Sereno MI, Dick F (2017) Functional and quantitative MRI
760 mapping of somatomotor representations of human supralaryngeal vocal tract. Cerebral
761 Cortex 27:265–278.
762 Casey BJ et al. (2018) The Adolescent Brain Cognitive Development (ABCD) study: Imaging
763 acquisition across 21 sites. Developmental Cognitive Neuroscience 32:43–54.
764 Clouchoux C, Coulon O, Anton JL, Mangin JF, Régis J (2006) A new cortical surface parcellation
765 model and its automatic implementation. In: Lecture Notes in Computer Science
766 (including subseries Lecture Notes in Artificial Intelligence and Lecture Notes in
767 Bioinformatics), pp 193–200. Springer, Berlin, Heidelberg.
768 Coulon O, Pizzagalli F, Operto G, Auzias G, Delon-Martin C, Dojat M (2011) Two new stable
769 anatomical landmarks on the Central Sulcus: Definition, automatic detection, and their
770 relationship with primary motor functions of the hand. In: Proceedings of the Annual
771 International Conference of the IEEE Engineering in Medicine and Biology Society, EMBS,
772 pp 7795–7798. IEEE.
773 Croxson PL, Forkel SJ, Cerliani L, Thiebaut De Schotten M (2018) Structural variability across
774 the primate brain: A cross-species comparison. Cerebral Cortex 28:3829–3841.
775 Derrfuss J, Vogt VL, Fiebach CJ, Von Cramon DY, Tittgemeyer M (2012) Functional organization
776 of the left inferior precentral sulcus: Dissociating the inferior frontal eye field and the
777 inferior frontal junction. NeuroImage 59:3829–3837.
778 Dorsaint-Pierre R, Penhune VB, Watkins KE, Neelin P, Lerch JP, Bouffard M, Zatorre RJ (2006)
779 Asymmetries of the planum temporale and Heschl's gyrus: Relationship to language
780 lateralization. Brain 129:1164–1176.
781 Eichert N, Papp D, Mars RB, Watkins KE (2020a) Mapping human laryngeal motor cortex during
782 vocalization. bioRxiv:2020.02.20.958314.

783 Eichert N, Robinson EC, Bryant KL, Jbabdi S, Jenkinson M, Li L, Krug K, Watkins KE, Mars RB
784 (2020b) Cross-species cortical alignment identifies different types of neuroanatomical
785 reorganization in higher primates. bioRxiv (https://doi.org/101101/645234).
786 Fischl B, Dale AM (2000) Measuring the thickness of the human cerebral cortex from magnetic
787 resonance images. Proceedings of the National Academy of Sciences of the United States
788 of America 97:11050–11055.
789 Fischl B, Sereno MI, Tootell RBH, Dale AM (1999) High-resolution intersubject averaging and a
790 coordinate system for the cortical surface. Human Brain Mapping 8:272–284.
791 Fonov V, Evans AC, Botteron K, Almli CR, McKinstry RC, Collins DL (2011) Unbiased average age-
792 appropriate atlases for pediatric studies. NeuroImage 54:313–327.
793 Foundas AL, Leonard CM, Gilmore RL, Fennell EB, Heilman KM (1996) Pars triangularis
794 asymmetry and language dominance. Proceedings of the National Academy of Sciences
795 of the United States of America 93:719–722.
796 Germann J, Chakravarty MM, Collins LD, Petrides M (2019) Tight coupling between
797 morphological features of the central sulcus and somatomotor body representations: A
798 combined anatomical and functional MRI study. Cerebral Cortex.
799 Germann J, Robbins S, Halsband U, Petrides M (2005) Precentral sulcal complex of the human
800 brain: Morphology and statistical probability maps. Journal of Comparative Neurology
801 493:334–356.
802 Glasser MF, Smith SM, Marcus DS, Andersson JLR, Auerbach EJ, Behrens TEJ, Coalson TS, Harms
803 MP, Jenkinson M, Moeller S, Robinson EC, Sotiropoulos SN, Xu J, Yacoub E, Ugurbil K, Van
804 Essen DC (2016) The Human Connectome Project's neuroimaging approach. Nature
805 Neuroscience 19:1175–1187.
806 Glasser MF, Sotiropoulos SN, Wilson JA, Coalson TS, Fischl B, Andersson JL, Xu J, Jbabdi S,

807 Webster M, Polimeni JR, Van Essen DC, Jenkinson M (2013) The minimal preprocessing
808 pipelines for the Human Connectome Project. NeuroImage 80:105–124.
809 Grabski K, Lamalle L, Vilain C, Schwartz JL, Vallée N, Tropres I, Baciu M, Le Bas JF, Sato M (2012)
810 Functional MRI assessment of orofacial articulators: Neural correlates of lip, jaw, larynx,
811 and tongue movements. Human Brain Mapping 33:2306–2321.
812 Hickok G, Lawrence Small S, Hillert DG (2016) Neurobiology of Language. Igarss 2014:1188.
813 Hitzig E, Fritsch GT (1870) Über die elektrische Erregbarkeit des Grosshirns. Arch Anat
814 Physiol:300–332.
815 Jackson J. (1863) Convulsive spasms of the right hand and arm preceding epileptic seizures.
816 Jakobsen E, Liem F, Klados MA, Bayrak Ş, Petrides M, Margulies DS (2018) Automated
817 individual-level parcellation of Broca's region based on functional connectivity.
818 NeuroImage 170:41–53.
819 Jarvis ED (2019) Evolution of vocal learning and spoken language. Science 366:50–54.
820 Jenkinson M (2003) Fast, automated, N-dimensional phase-unwrapping algorithm. Magnetic
821 Resonance in Medicine 49:193–197.
822 Jenkinson M, Bannister P, Brady M, Smith S (2002) Improved optimization for the robust and
823 accurate linear registration and motion correction of brain images. NeuroImage 17:825–
824 841.
825 Jenkinson M, Smith S (2001) A global optimisation method for robust affine registration of
826 brain images. Medical Image Analysis 5:143–156.
827 Josse G, Tzourio-Mazoyer N (2004) Hemispheric specialization for language. Brain Research
828 Reviews 44:1–12.
829 Klein A, Ghosh SS, Avants B, Yeo BTT, Fischl B, Ardekani B, Gee JC, Mann JJ, Parsey R V. (2010)
830 Evaluation of volume-based and surface-based brain image registration methods.

831 NeuroImage 51:214–220.

832 Miller MB, Van Horn JD, Wolford GL, Handy TC, Valsangkar-smyth M, Inati S, Grafton S,
833 Gazzaniga MS (2002) Extensive individual differences in brain activations associated with
834 episodic retrieval are reliable over time. Journal of Cognitive Neuroscience 14:1200–1214.

835 Nieto-Castañón A, Fedorenko E (2012) Subject-specific functional localizers increase sensitivity
836 and functional resolution of multi-subject analyses. NeuroImage 63:1646–1669.

837 Olthoff A, Baudewig J, Kruse E, Dechent P (2008) Cortical Sensorimotor Control in Vocalization:
838 A Functional Magnetic Resonance Imaging Study. The Laryngoscope 118:2091–2096.

839 Penfield W, Boldrey E (1937) Somatic motor and sensory representation in the cerebral cortex
840 of man as studied by electrical stimulation. Brain 60:389–443.

841 Petrides M (2012) The human cerebral cortex. An MRI atlas of the sulci and gyri in MNI
842 stereotaxic space. :168.

843 Petrides M (2019) Atlas of the morphology of the human cerebral cortex on the average MNI
844 brain. New York: Academic Press.

845 Price CJ (2000) The anatomy of language: Contributions from functional neuroimaging. Journal
846 of Anatomy 197:335–359.

847 Ribas GC (2010) The cerebral sulci and gyri. Neurosurgical Focus 28.

848 Robinson EC, Jbabdi S, Glasser MF, Andersson J, Burgess GC, Harms MP, Smith SM, Van Essen
849 DC, Jenkinson M (2014) MSM: A new flexible framework for multimodal surface matching.
850 NeuroImage 100:414–426.

851 Simonyan K (2014) The laryngeal motor cortex: Its organization and connectivity. Current
852 Opinion in Neurobiology 28:15–21.

853 Smith S, Duff E, Groves A, Nichols TE, Jbabdi S, Westlye LT, Tamnes CK, Engvig A, Walhovd KB,
854 Fjell AM, Johansen-Berg H, Douaud G (2019) Structural variability in the human brain

855 reflects fine-grained functional architecture at the population level. The Journal of
856 Neuroscience 39:6136–6149.
857 Sprung-Much T, Petrides M (2018) Morphological patterns and spatial probability maps of two
858 defining sulci of the posterior ventrolateral frontal cortex of the human brain: the sulcus
859 diagonalis and the anterior ascending ramus of the lateral fissure. Brain Structure and
860 Function 223:4125–4152.
861 Sprung-Much T, Petrides M (2019) Morphology and spatial probability maps of the horizontal
862 ascending ramus of the lateral fissure. Cerebral Cortex 00:1–17.
863 Takerkart S, Auzias G, Brun L, Coulon O (2015) Mapping cortical shape differences using a
864 searchlight approach based on classification of sulcal pit graphs. In: Proceedings -
865 International Symposium on Biomedical Imaging, pp 1514–1517. IEEE.
866 Uğurbil K et al. (2013) Pushing spatial and temporal resolution for functional and diffusion MRI
867 in the Human Connectome Project. NeuroImage 80:80–104.
868 Van Essen DC, Smith SM, Barch DM, Behrens TEJJ, Yacoub E, Ugurbil K (2013) The WU-Minn
869 Human Connectome Project: An overview. NeuroImage 80:62–79.
870 Vigneau M, Beaucousin V, Hervé PY, Duffau H, Crivello F, Houdé O, Mazoyer B, Tzourio-
871 Mazoyer N (2006) Meta-analyzing left hemisphere language areas: Phonology, semantics,
872 and sentence processing. NeuroImage 30:1414–1432.
873 Vogt C, Vogt O (1919) Allgemeinere Ergebnisse unserer Hirnforschung. Journal für Psychologie
874 und Neurologie.
875 Weiskopf N, Suckling J, Williams G, Correia M. MM, Inkster B, Tait R, Ooi C, Bullmore T. ET, Lutti
876 A (2013) Quantitative multi-parameter mapping of R1, PD*, MT, and R2* at 3T: A multi-
877 center validation. Frontiers in Neuroscience 7:95.
878 Woo CW, Krishnan A, Wager TD (2014) Cluster-extent based thresholding in fMRI analyses:

879 Pitfalls and recommendations. NeuroImage 91:412–419.

880 Woolrich MW, Ripley BD, Brady M, Smith SM (2001) Temporal autocorrelation in univariate

881 linear modeling of FMRI data. NeuroImage 14:1370–1386.

882 Yousry TA, U.D. Schmid HA, Schmidt D, Peraud A, Buettner A, Winkler P (1997) Localization of

883 the motor hand area to a knob on the precentral gyrus. Brain 120:141–157.

884 Zhang H, Schneider T, Wheeler-Kingshott CA, Alexander DC (2012) NODDI: Practical in vivo

885 neurite orientation dispersion and density imaging of the human brain. NeuroImage

886 61:1000–1016.

887 Zlatkina V, Amiez C, Petrides M (2016) The postcentral sulcal complex and the transverse

888 postcentral sulcus and their relation to sensorimotor functional organization. European

889 Journal of Neuroscience 43:1268–1283.

890 Zlatkina V, Petrides M (2010) Morphological patterns of the postcentral sulcus in the human

891 brain. Journal of Comparative Neurology 518:3701–3724.

892